Atmosphere-Ocean

ISSN: 0705-5900 (Print) 1480-9214 (Online) Journal homepage: https://www.tandfonline.com/loi/tato20

The Impact of Cloud Representation on the Sub-Seasonal Forecasts of Atmospheric Teleconnections and Preferred Circulation Regimes in the Northern Hemisphere

Cristiana Stan & David M. Straus

To cite this article: Cristiana Stan & David M. Straus (2019) The Impact of Cloud Representation on the Sub-Seasonal Forecasts of Atmospheric Teleconnections and Preferred Circulation Regimes in the Northern Hemisphere, Atmosphere-Ocean, 57:3, 233-248, DOI: 10.1080/07055900.2019.1590178

To link to this article: https://doi.org/10.1080/07055900.2019.1590178

Published online: 24 May 2019.

The Impact of Cloud Representation on the Sub-Seasonal Forecasts of Atmospheric Teleconnections and Preferred Circulation Regimes in the Northern Hemisphere

Cristiana Stan* and David M. Straus

Department of Atmospheric, Oceanic and Earth Sciences, George Mason University, Fairfax, Virginia, United States

[Original manuscript received 20 July 2018; accepted 2 February 2019]

ABSTRACT *The impact of cloud representation on the simulation of mid-latitude recurrent large-scale flows and forecast skill of mid-latitude atmospheric teleconnections is evaluated using the Community Climate System Model, version 4 (CCSM4), and the super-parameterized CCSM4 (SP-CCSM4). Patterns of low-level atmospheric circulation anomalies and convection associated with the Madden–Julian oscillation (MJO) are affected by the method used for the representation of cloud processes. The configuration of the model using super-parameterization for the representation of cloud processes produces MJO-related patterns that agree better with observations than the configuration of the model using a conventional cloud parameterization scheme. The recurrent circulation regimes of the mid-latitudes are also sensitive to the representation of cloud processes. In the North Atlantic sector, the inability of CCSM4 to simulate the Scandinavian blocking regime is corrected in the super-parameterized version of the model. In the North Pacific sector, the strength of the clustering (measured by a variance ratio) is too large in CCSM4 compared with observations and SP-CCSM4. The SP-CCSM4 model has better forecast skill for the MJO amplitude and phase than the model with conventional representation of moist convective processes. In turn, the improved forecast skill of the super-parameterized model results in better forecast skill for mid-latitude teleconnections in 500 hPa geopotential height anomalies forced by the MJO convection.*

RÉSUMÉ *[Traduit par la rédaction] Nous évaluons l'impact de la représentation des nuages sur la simulation de courants récurrents de grande échelle et sur la capacité de prévoir des téléconnexions atmosphériques, et ce, aux latitudes moyennes, à l'aide de la version 4 du Community Climate System Model (CCSM4) et du CCSM4 avec super-paramétrisation (SP-CCSM4). La méthode choisie pour représenter l'évolution des nuages influe sur la configuration des anomalies de la circulation atmosphérique à basse altitude et sur la convection associées à l'oscillation de Madden–Julian (OMJ). L'utilisation de super-paramétrisation pour représenter l'évolution des nuages génère une répartition des valeurs liées à l'OMJ qui concorde mieux avec les observations que l'application classique de paramétrisation des nuages. Les régimes de circulation récurrents des latitudes moyennes sont également sensibles à la représentation des processus relatifs aux nuages. Dans le secteur de l'Atlantique Nord, l'incapacité du CCSM4 à simuler le régime de blocage scandinave est corrigée par la super-paramétrisation. Dans le secteur du Pacifique Nord, l'intensité du regroupement (rapport de variances) est trop grande dans le CCSM4 par rapport aux observations et au SP-CCSM4. Le modèle SP-CCSM4 montre une meilleure capacité de prévision de l'amplitude et de la phase de l'oscillation de Madden–Julian que le modèle utilisant une représentation conventionnelle du processus convectif humide. En outre, l'amélioration de la capacité de prévision que permet la super-paramétrisation se traduit par une capacité supérieure de prévision des téléconnexions aux latitudes moyennes en ce qui a trait aux anomalies de hauteur géopotentielle à 500 hPa sur lesquelles influe la convection associée à l'oscillation de Madden–Julian.*

KEYWORDS convective parameterization; super-parameterization; MJO; atmospheric teleconnections

1 Introduction

A significant fraction of recurring anomalies observed in the large-scale atmospheric circulation of the northern hemisphere mid-latitudes can be related to the intra-seasonal variability of the tropics (e.g., Cassou, 2008; Hoskins & Karoly, 1981; Kim, Webster, Toma, & Kim, 2014; Knutson & Weickmann, 1987). During boreal winter, these atmospheric teleconnections tend to be favoured by particular patterns of convective activity associated with the Madden–Julian Oscillation (MJO). Previous studies showed that current operational models have improved the forecast skill of the MJO (Hudson, Marshall, Yin, Alves, & Hendon, 2013; Rashid, Hendon, Weehler, &

*Corresponding author's email: cstan@gmu.edu

Alves, 2011; Seo et al., 2009; Vitart, 2014; Vitart & Molteni, 2010; Vitart, Woolnough, Balmaseda, & Tompkins, 2007; Wang, Hung, Weaver, Kumar, & Fu, 2014; Wu et al., 2016). Some of these studies attribute the improvements to better initialization methodologies (e.g., Kang, Jang, & Almazroui, 2014; Kang & King, 2009); others emphasize the role of coupled air–sea interactions (Fu et al., 2013); still others report that a combination of both contributed to the improvement in skill (Hudson et al., 2013).

The impact of cloud representation on the simulation of the MJO in free climate simulations with super-parameterization has been previously reported (e.g., DeMott, Stan, Branson, & Randall, 2014; Jiang et al., 2014; Khairoutdinov, Randall, & DeMott, 2005; Stan et al., 2010; Thayer-Calder & Randall, 2009). In a super-parameterized atmospheric model, tropical convection moistens the entire troposphere and further produces intense latent heating, which excites the large-scale circulation associated with the MJO (Thayer-Calder & Randall, 2009). Super-parameterization simulates the MJO with a realistic period and eastward propagation across the Maritime Continent (Stan et al., 2010). These capabilities of simulating realistic variability associated with the MJO have the potential for improving the model's prediction skill. However, the impact of super-parameterization on the MJO prediction skill has yet to be determined. In a short-term hindcast experiment during two MJO events within the Year of Tropical Convection (Waliser et al., 2012), the super-parameterized model described by Thayer-Calder and Randall (2009) was consistently wetter than observations for the convective phase (Xavier et al., 2015). The first objective of this study is to compare the forecast skill for MJO of a model using two methods for the representation of moist convective processes: conventional parameterization and super-parameterization.

Using various approaches, previous studies have suggested an improvement in forecast skill for mid-latitude teleconnection patterns with a reduction in errors in the simulation of tropical variability. Ferranti, Palmer, Molteni, and Klinker (1990) and Jung, Miller, and Palmer (2010) showed an improvement in the extra-tropical deterministic forecast skill and Vitart and Molteni (2010) showed that the MJO forecast skill has a significant impact on the weekly mean probabilistic skill scores in the northern hemisphere for the time range of 19–25 days.

The second objective of this manuscript is to evaluate the impact of super-parameterization on the simulation and forecast skill for mid-latitude recurrent states and tropical teleconnection patterns on time scales between weather and climate. Recurrent states are identified using cluster analysis, while the teleconnection patterns are obtained as composites during particular phases of the MJO. These two classes of mid-latitude states are not disconnected: tropical forcing associated with the MJO is known to change the frequency of occurrence of circulation regimes in the Euro–Atlantic region (Cassou, 2008; Lin, Derome, & Brunet, 2009; Yadav & Straus, 2017).

Vitart (2017) showed that models in the subseasonal-to-seasonal (S2S) database (Vitart et al., 2017) have a lower prediction skill for the MJO teleconnections in the northern extra-tropics than for the MJO itself.

In Section 2, the models and datasets used in this study are described, and the numerical experiments are explained. Section 3 presents the main findings of the study. In Section 4, results are summarized and their significance for sub-seasonal prediction systems are discussed.

2 Description of model, datasets and numerical experiments

The model used in this study was the Community Climate System Model, version 4 (CCSM4) (Gent et al., 2011), with two methods for the representation of moist convection. In the first method, clouds are represented using a conventional parameterization scheme, with different approaches for deep convection (Neale, Richter, & Jochum, 2008; Richter & Rasch, 2008; Zhang & McFarlane, 1995) and shallow convection (Hack, 1994). In the second method, referred to as super-parameterization (Grabowski, 2004), a two-dimensional (2D) cloud resolving model (CRM) is embedded in each grid column of the atmospheric model as described by Grabowski (2001) and Khairoutdinov and Randall (2001). The horizontal resolution of the model's components is 1° and the grid spacing in the east–west direction of the CRM is 3 km. The simulation of mean and climate variability by the super-parameterized version of CCSM4, referred to as SP-CCSM4, was documented by Stan and Xu (2014).

The two versions of the model are used to produce two sets of re-forecasts. The ensemble re-forecasts are initialized on 1 November every year between 1982 and 2009 and consists of five members. Initial conditions for each ensemble member are 1 day apart and are centred on 1 November. The initial conditions are from the Climate Forecast System Reanalysis (CFSR) documented by Saha et al. (2010). Each re-forecast spans 12 months, and in this study only November–February months are analyzed.

The models' prediction skill is evaluated by comparing each set of re-forecasts to each other and observations. The National Oceanic and Atmospheric Administration's (NOAA) interpolated outgoing longwave radiation (OLR) dataset (Liebmann & Smith, 1996) is used as a proxy for tropical convection. The other parameters used for the evaluation of dynamical variables are taken from the European Centre for Medium-range Weather Forecasts interim reanalysis (ERA-Interim; Dee et al., 2011).

3 Results

a *MJO Forecast Skill*

The anomalies and the Wheeler Hendon Real-time Multivariate MJO index (RMM; Wheeler & Hendon, 2014) of the re-forecasts are computed by projecting the model forecast anomalies onto the observed MJO's empirical orthogonal function (EOF) patterns following the framework described by Gottschalck et al. (2010). The low frequency variability

associated with the El Niño Southern–Oscillation (ENSO) has been removed from the forecast anomalies by subtracting the 120-day running mean from each day of the forecast. The prediction skill of MJO is estimated by the bivariate anomaly correlation coefficient, bivariate root mean square error (RMSE) and phase angle error following Kim et al. (2014). A comparison of these metrics between the model with conventional representation of convection (CCSM) and the super-parameterized version of the model (SP-CCSM) is shown in Fig. 1. The relatively small value of the anomaly correlation coefficient (Fig. 1a) compared with operational forecast systems (e.g., Kim et al., 2014) can be attributed to the limited sample size of initial conditions. This initialization method is more suitable for seasonal forecasts than for sub-seasonal time scales. For example, Lin, Brunet, and Derome (2008) found that the role of initial conditions in the first two weeks is crucial for the MJO forecast skill. The initial value of anomaly correlation in SP-CCSM is larger than in CCSM. In the first two weeks, both models display a decrease in forecast skill at the same rate. In the third week, CCSM experiences a faster decrease in skill than SP-CCSM, which shows some skill up to 30 days. In the first week, the RMSE of CCSM is about two times larger than in SP-CCSM, and the two models reach saturation by the end of third week (Fig. 1b). The phase error is also much larger in CCSM than in SP-CCSM (Fig. 1c). In CCSM, the phase error is positive suggesting a faster than observed propagation, whereas in SP-CCSM the phase speed error is slightly negative, suggesting a somewhat slower propagation speed.

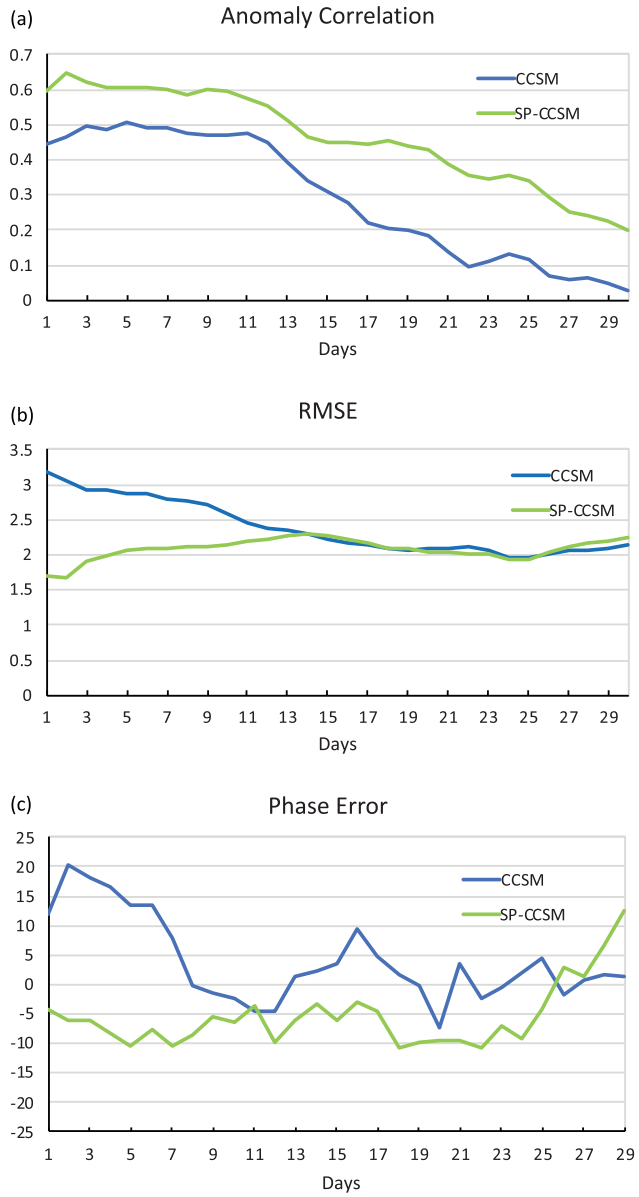

Fig. 1 (a) Bivariate correlation coefficient, (b) bivariate RMSE of ensemble mean, and (c) phase angle error between the observed and predicted RMMs relative to observations as a function of forecast lead day in CCSM (blue) and SP-CCSM (green).

To illustrate some dynamical and thermodynamical characteristics of the re-forecasts, two MJO events are compared: one event that occurred in November 1984 (Fig. 2), and the second event took place in November 1996 (Fig. 3). The 1984 event was documented by Cunningham and Cavalcanti (2006) in connection with an extreme precipitation event over southeastern Brazil. The second event is selected because the two models forecast it with comparable skill.

For the November 1984 MJO event, the CCSM model maintains the 850 hPa westerly wind and OLR anomalies (a proxy for convection) reminiscent of a previous event. It also generates a second MJO event around mid-November, but this event does not propagate across the Maritime Continent. In SP-CCSM, the pattern of westerlies shows a closer resemblance to the verification than CCSM, and overall the pattern correlation of zonal wind anomalies is higher in SP-CCSM (0.33) than in CCSM (0.08). Both models forecast weaker than observed convective activity during this MJO event. The phase evolution of the RMM index in SP-CCSM is consistent with observations for most of the ensemble members and ensemble mean, whereas CCSM forecasts remain clustered in the western hemisphere.

For the November 1996 MJO event, both models have good forecast skill for the 850 hPa zonal wind anomalies throughout the event, with a higher overall correlation for SP-CCSM (0.36) than CCSM (0.21). The amplitude of convective anomalies is realistic in the first week and then decreases in both models. The phase evolution of the RMM index is consistent with observations in both models, suggesting a realistic propagation of the MJO in the models.

It is interesting to notice that in observations the 1984 event is dominated by a clear signal in the convective activity, whereas the 1996 event is dominated by a coherent signal in the wind. This could explain the better forecast skill of CCSM for the 1996 event relative to the 1984 event. Both models show no forecast skill for OLR anomalies during the 1984 event. Correlation coefficients for all years are shown in Table 1. There are also years when super-parameterization improves the forecast of convective activity compared with

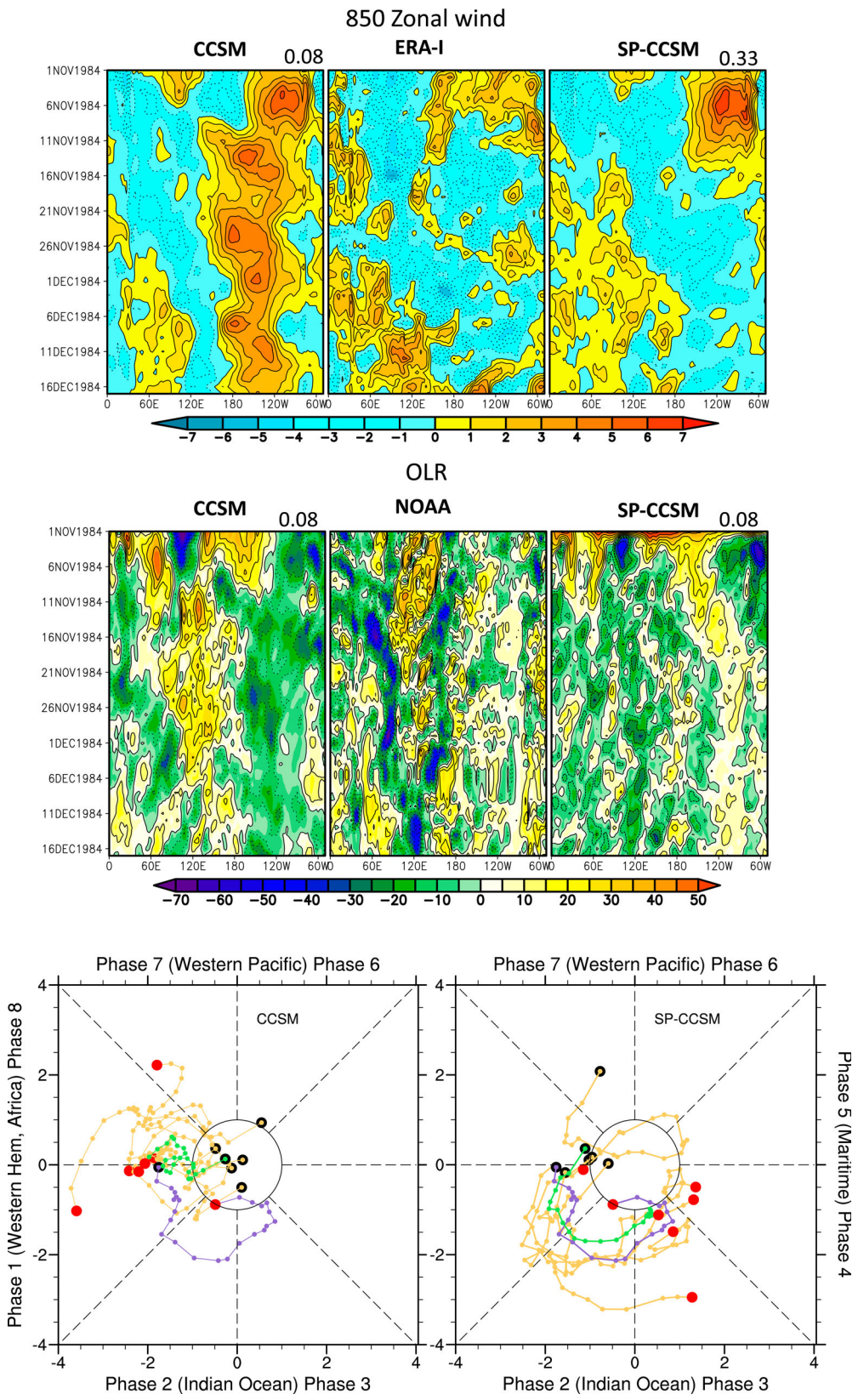

Fig. 2 850 hPa zonal wind and OLR daily anomaly for observations and model ensemble average. Phase diagram for observations (purple), ensemble members (orange), and ensemble average (green) of CCSM and SP-CCSM re-forecasts initialized on 1 November 1984. Dots represent every day from the forecast starting date (black) up to 25 days (red). The pattern correlation of the SP-CCSM and CCSM daily anomalies with observations are indicated in the right corner.

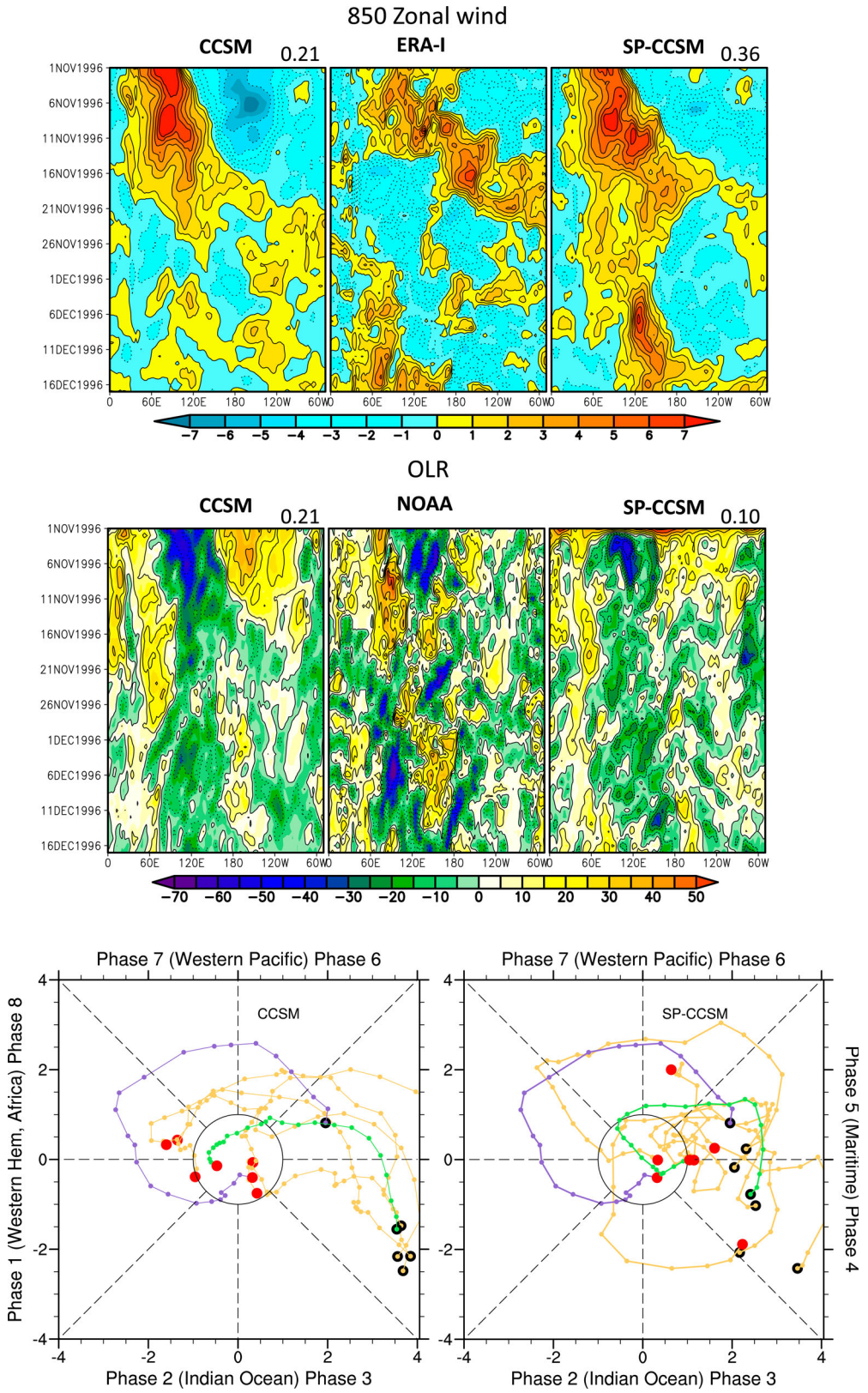

Fig. 3 As in Fig. 2, but for the re-forecast initialized on 1 November 1996.

TABLE 1. The pattern correlation of OLR and 850 hPa zonal wind (U850) anomalies between observations and ensemble mean forecast based on 1 November to 17 December of each forecasted year. Values when the correlation coefficient of SP-CCSM is 50% higher than CCSM are in bold.

	CCSM		SP-CCSM	
Year	OLR	U850	OLR	U850
1983	0.07	0.27	**0.16**	**0.37**
1984	0.08	0.08	0.08	**0.33**
1985	0.05	0.42	**0.13**	0.52
1986	0.24	0.51	0.20	0.54
1987	0.33	0.63	0.38	0.57
1988	0.11	0.23	0.10	**0.36**
1989	0.13	0.06	0.13	**0.21**
1990	0.15	0.38	0.00	0.20
1991	−0.08	−0.09	0.02	−0.05
1992	0.06	−0.16	0.02	0.07
1993	0.16	0.45	**0.24**	0.40
1994	0.10	0.46	**0.17**	0.46
1995	0.11	0.36	0.11	0.37
1996	0.21	0.21	0.10	0.36
1997	−0.08	−0.36	**0.21**	**0.44**
1998	0.26	0.49	0.36	0.67
1999	0.20	0.49	0.14	0.54
2000	0.20	0.20	0.19	0.12
2001	0.09	0.38	0.02	0.40
2002	0.10	0.17	**0.20**	**0.45**
2003	0.00	0.05	**0.10**	**0.21**
2004	0.33	0.09	0.25	0.13
2005	0.17	0.43	0.19	0.27
2006	−0.03	0.03	**0.16**	**0.43**
2007	0.18	0.45	0.18	0.37
2008	0.15	0.37	0.15	0.27
Average	*0.13*	*0.26*	*0.15*	*0.36*

conventional parameterization. Overall, the forecast skill of 850 hPa zonal wind anomalies is higher than the forecast skill of OLR anomalies for both models, and the mean correlation for the OLR anomalies is comparable for the two models.

b *Northern Hemisphere Mid-Latitude Circulation Flow*

The mid-latitude circulation flow in the northern hemisphere winter is examined using a cluster analysis method based on the k means partitioning algorithm (e.g., Michelangeli, Vautard, & Legras, 1995; Straus, Corti, & Molteni, 2007). Cluster analysis is applied separately to the Euro-Atlantic ($90°\text{W} - 30°\text{E}$, $20° - 80°\text{N}$) and North Pacific ($150° - 330°\text{E}$, $20° - 80°\text{N}$) regions. The circulation regimes are generated using daily anomalies of 500 hPa geopotential height (Z500) filtered to retain low frequency variability with periods longer than 10 days, and clustering is formed on a reduced space defined by the six leading EOFs of the anomalies. Daily maps of Z500 for the winter period of 16 December to 31 March for the 27 years spanning 1982–2008 in the model simulations and the ERA-Interim reanalyses were used in the cluster analysis

The algorithm partitions all data points in the reduced principal component (PC) space to one of k clusters, where k must be chosen a priori. Each cluster is characterized by a centroid (the average position of all the cluster members) and an intracluster variance about that centroid. The overall strength of the clustering is measured by the variance ratio, defined as the ratio of the variance of the centroids to the average intracluster variance. Significance is assessed by comparing this variance ratio to those found when the cluster analysis is applied to 100 surrogate datasets. Each surrogate dataset is the same size as the original dataset but is generated by six stochastic processes, each process being Gaussian but adjusted to have the same autocorrelation properties as one of the original PCs. The percentage of surrogate datasets for which the variance ratio is less than that of the original dataset gives a confidence level. For further details of the generation of surrogate datasets and the meaning of the variance ratio, see Straus (2010) and Straus, Molteni, and Corti (2017).

For the Euro-Atlantic sector, many studies (including that of Cassou, 2008) find consistent results for $k = 4$. We also find a confidence level exceeding 99% once k is equal to or greater than 4. The maps corresponding to the cluster centroids in the Euro-Atlantic sector are shown in Fig. 4 for both models and the reanalysis. The pattern correlation between each model centroid and its reanalysis counterpart is indicated in the titles. The circulation regimes correspond to the positive and negative phases of the North Atlantic Oscillation, referred to as NAO+ and NAO−, Scandinavian blocking (ScBL), and Atlantic Ridge (AtRd), also identified by Ferranti, Corti, and Janousek (2015). In the models, the positive geopotential height anomaly of the NAO+ pattern is distorted compared with the reanalysis pattern, although the SP-CCSM has a higher pattern correlation with the reanalysis (0.88) than does the CCSM model (0.70). The NAO− pattern is clearly better simulated by the SP-CCSM (correlation of 0.93) than the CCSM (correlation of 0.76).

The positive height anomalies over Greenland associated with the observed ScBL pattern are captured by the SP-CCSM, whereas in the CCSM simulation the sign of the geopotential height anomalies is reversed compared with observations. (Note the negative pattern correlation of the CCSM (−0.56) compared with 0.80 for the SP-CCSM.) Because the centroid is significantly different from observations it is likely that a misrepresentation of physical processes in the model is causing this error. Because the only difference between the two models is in the representation of clouds, we speculate that the differences in the simulation of convective activity in the tropics described in Section 3.b play a role. Davini, von Hardenberg, and Corti (2015) noticed that changes in the tropical Atlantic sea surface temperature (SST) have a larger impact on the atmospheric blocking over the Euro-Atlantic sector than do changes in the mid-latitude SST. They attribute this impact to a Gill-like response produced by the latent heat released by the precipitation induced by the SST anomaly. The anomalies in the upper tropospheric tropical circulation affect the position of the jet stream, which influences the propagation and breaking of Rossby waves tightly coupled with the occurrence of blocking. In the case of CCSM and SP-CCSM, precipitation and

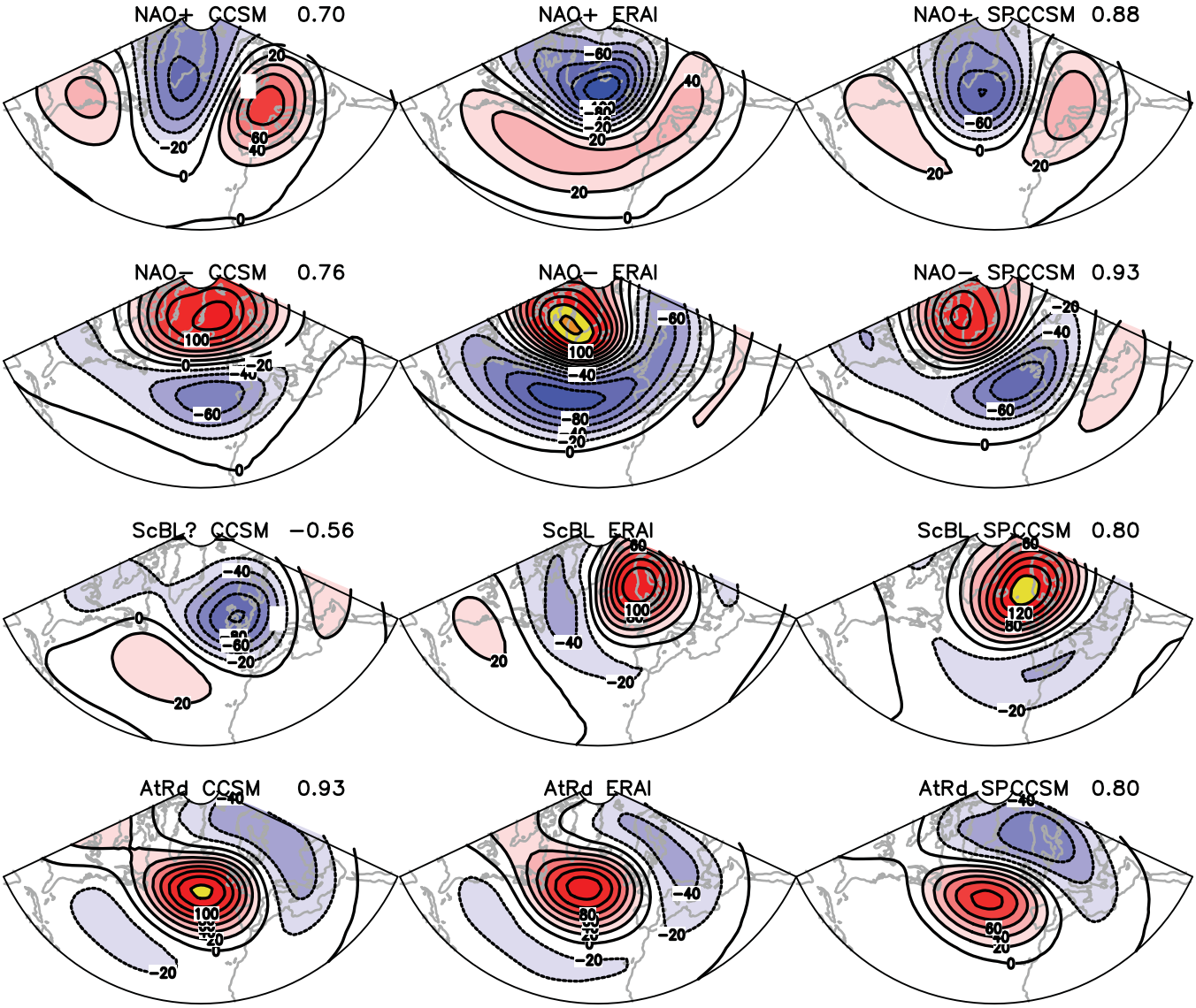

Fig. 4 Maps of the Euro-Atlantic circulation flow regimes (centroids of the clusters): NAO+, NAO−, Scandinavian Blocking (ScBL), and Atlantic Ridge (AtRd) shown in rows; CCSM (left), ERA-Interim (middle), and SP-CCSM (right). The pattern correlation of the SP-CCSM and CCSM maps with the ERA-Interim maps are indicated in the titles.

the associated latent heat release differs between the two models. Biases in the Greenland blocking have also been associated with biases in the simulation of storm tracks (Zappa, Masato, Woollings, & Hodges, 2013) on which convective parameterizations can have an impact (Park & Bretherton, 2009). However, both CCSM and SP-CCSM have very similar biases in the simulation of storm tracks (not shown). The negative anomalies over Europe seen in observations are missed by both models.

The AtRd pattern is captured well by the models, with a slightly stronger amplitude and stronger pattern correlation in the model with conventional parameterization of clouds.

The variance ratio, shown in Table 2, indicates that the strength of the clustering is somewhat less in both models than in the observations.

For the North Pacific sector, the significance of the clustering is generally not as high. In order to achieve confidence levels over 95% for the observations, we need k to be at least 5. Thus we compared the 5-cluster set between the observations and the models. Within these sets, we found four

TABLE 2. Variance ratio of the 4-cluster set for the Euro-Atlantic region and the 5-cluster set for the North Pacific region, for the ERA-Interim reanalysis and the two models. (The variance ratio is defined as the ratio of the variance of the centroids to the average intra-cluster variance.)

	Euro-Atlantic	North Pacific
ERA-Interim	0.683	0.656
SP-CCSM	0.526	0.733
CCSM	0.523	0.821

common patterns, which are shown in Fig. 5. We refer to these patterns as the Arctic Low (ArcLo), Alaskan Block (AlkBl), Pacific Trough (PacTr), and Wave Train (WavTr). The pattern correlations between both models and the reanalysis are at least 0.85 except for the WavTr, for which the SP-CCSM pattern correlation is only 0.77, and the CCSM correlation 0.70. Other notable differences between the models and reanalysis are the CCSM ArcLo, in which the high over the North Pacific is weak, the AlkBl for SP-CCSM, in which the Alaskan high is shifted eastward, and the PacTr in the SP-CCSM, where the high over North America is shifted southward.

In order to indicate how representative the four patterns given in Fig. 5 are of the states going into each cluster, we have computed the probability distribution function (pdf) of the pattern correlation between each state and the cluster to which it is assigned. The pdfs for each cluster are given in a separate panel in Fig. 6, in which each panel has three lines for the three datasets: two models and the reanalysis. The pdfs generally peak near pattern correlations of 0.60 and higher, with almost no negative correlations. The AlkBl pdf is the narrowest in all datasets, and the WavTr the largest spread. Generally, the model and reanalysis pdfs agree with each other, the one exception being the high peak of the CCSM4 AlkBl.

Table 2 shows the variance ratio of the 4-cluster set for the Euro-Atlantic sector and the 5-cluster set for the North Pacific sector. Recalling that the variance ratio (ratio of the variance of the centroids to the average intra-cluster variance) gives a measure of the degree of clustering, we see that the reanalysis shows more clustering in the Euro-Atlantic than in the North

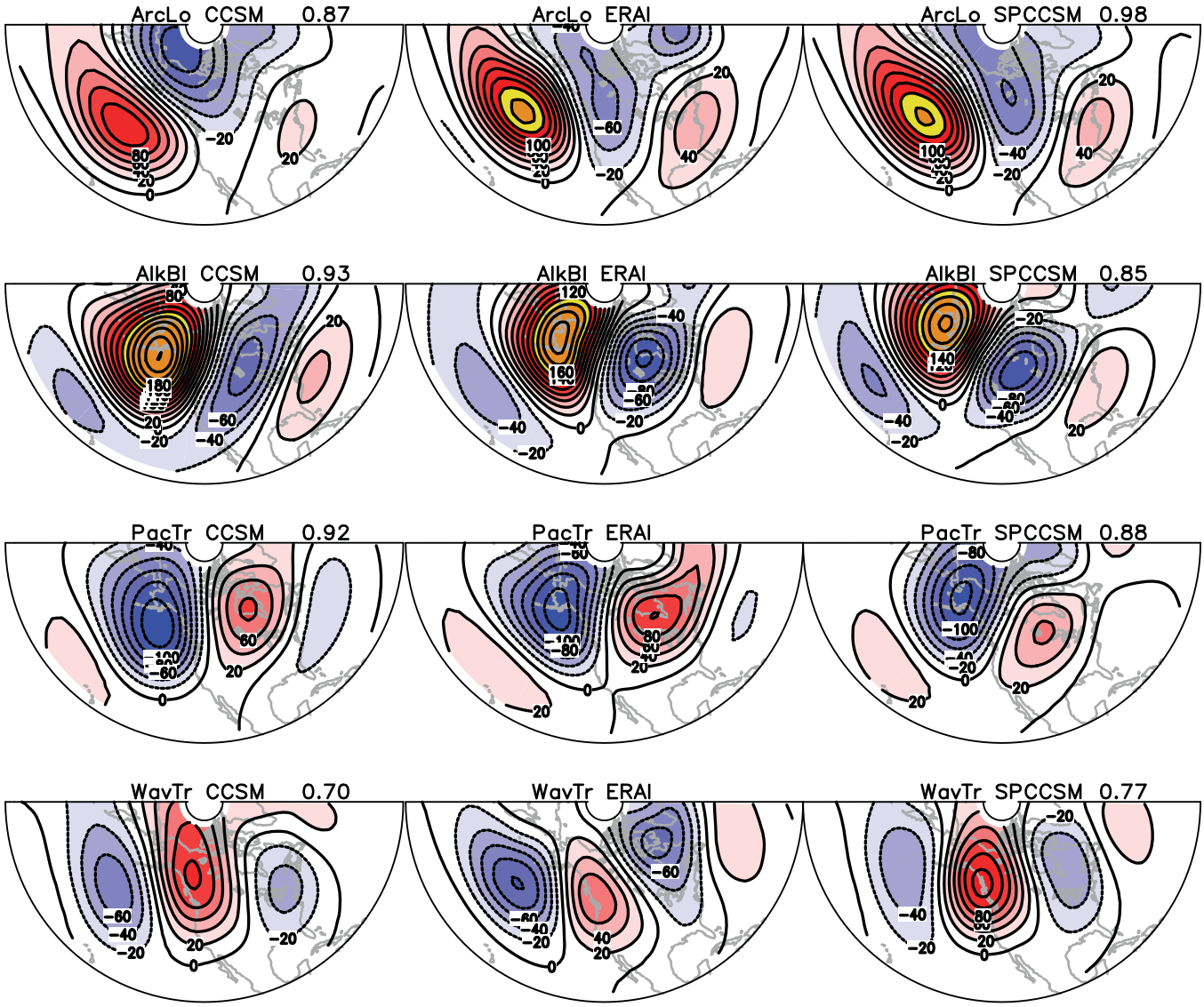

Fig. 5 Maps of the North Pacific circulation flow regimes (centroids of the clusters): Arctic Low (ArcLo), Alaskan Blocking (AlkBl), Pacific Trough (PacTr), and Wave Train (WavTr) shown in rows: CCSM (left), ERA-Interim (middle), and SP-CCSM (right). The pattern correlation of the SP-CCSM and CCSM maps with the ERA-Interim maps is indicated in the titles.

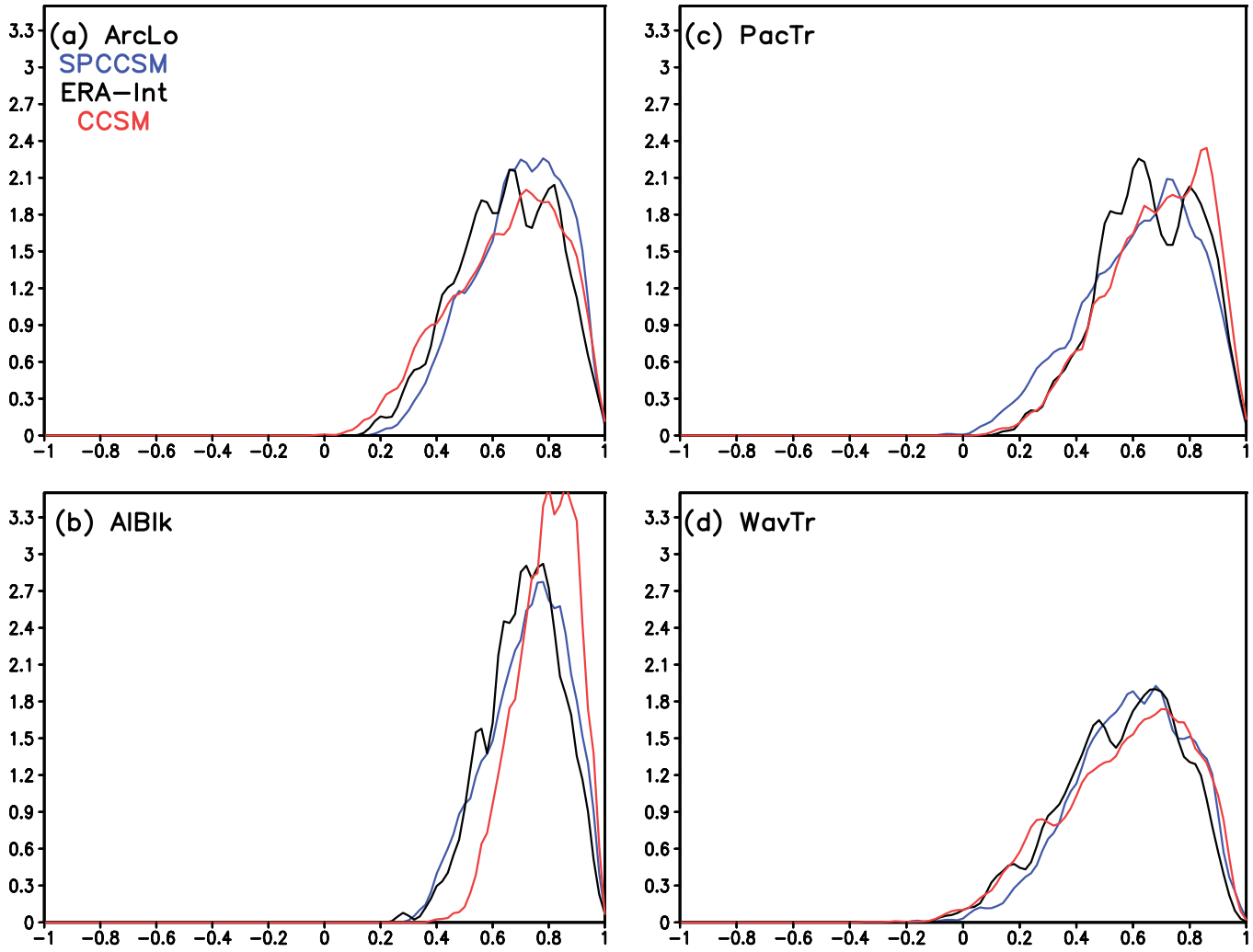

Fig. 6 Probability distribution function (pdf) of the pattern correlation of each state with the cluster (regime) centroid to which it is assigned for the North Pacific region: (a) Arctic Low (ArcLo); (b) Alaskan Block (AlkBl); (c) Pacific Trough (PacTr); and (d) Wave Train (WavTra). Blue curves for SP-CCSM, black for ERA-Interim, and red for CCSM. The pdfs were computed with a kernel density estimation and are normalized to have unit area.

Pacific, while the models show the opposite. The CCSM in particular is very highly clustered in the North Pacific.

c *Northern Hemisphere Mid-Latitude Teleconnection Forecast Skill*

The relationship between the tropical forcing associated with MJO convection and forecast skill of mid-latitude circulation is evaluated in the two models and compared with observations. Previous studies have shown that a dipole convection pattern associated with an MJO, with enhanced convection in the tropical Indian Ocean and reduced convection in the tropical western Pacific tends to be followed in 10–15 days by an NAO+ pattern in the mid-latitudes (Lin et al., 2009). The reverse dipole pattern with enhanced convection in the western Pacific and suppressed convection in the eastern Indian Ocean has been associated with positive geopotential height anomalies in the Gulf of Alaska (Tseng, Barnes, & Maloney, 2018).

The mid-latitude teleconnections are computed with respect to MJO convective activity located in the Indian Ocean (MJO phases 2 and 3) and in the western Pacific (MJO phases 6 and 7). The forecast skill of Z500 in the first four weeks lead time after the MJO convective activity is located in each of the two basins is shown in Figs 7–10. The location of convective activity is determined using the RMM index with values greater than or equal to two standard deviations, which is typical for strong MJO events (Kiladis et al., 2014). The RMM index used in the compositing can be model based (Figs 7 and 9) or observation based (Figs 8 and 10). The model-based calculation refers to the framework described in Section 3.a. Overall, the forecast skill of mid-latitude teleconnection patterns forced by MJO convection is better when the RMM index is computed using re-forecast anomalies rather than observed anomalies. The degradation of the skill for observation-only verification could be explained by the small sample size of initial conditions. It also suggests that small errors in the phase and/or location of MJO convection

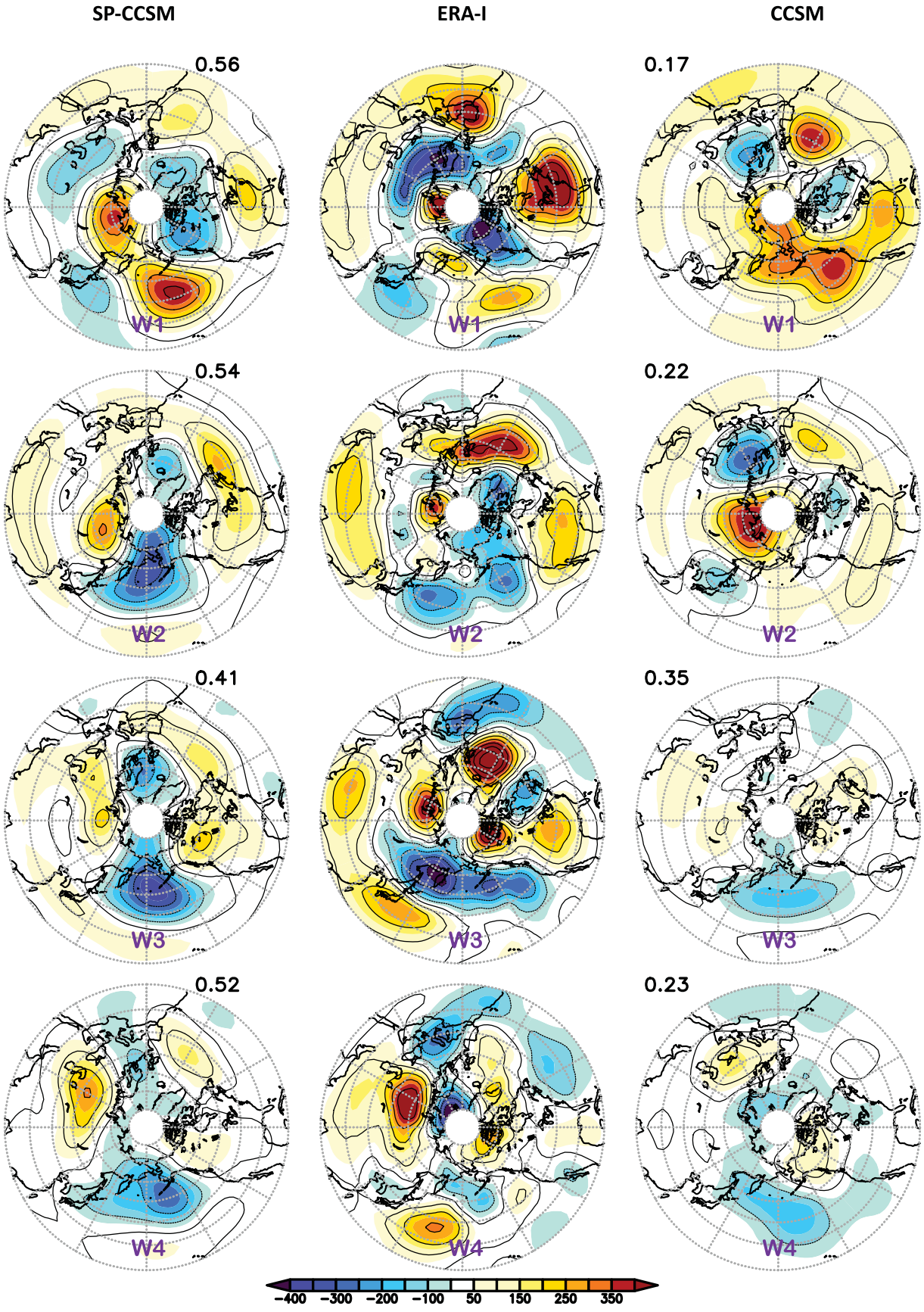

Fig. 7 Composites of 500 hPa geopotential height daily anomaly for days when active convective activity in the model is located over the Indian Ocean in SP-CCSM (left), ERA-Interim (middle), and CCSM (right) and lead time week 1 (W1) through week 4 (W4). The pattern correlation of the SP-CCSM and CCSM composite anomalies with the ERA-Interim composite anomalies are indicated on the left for SP-CCSM and right for CCSM.

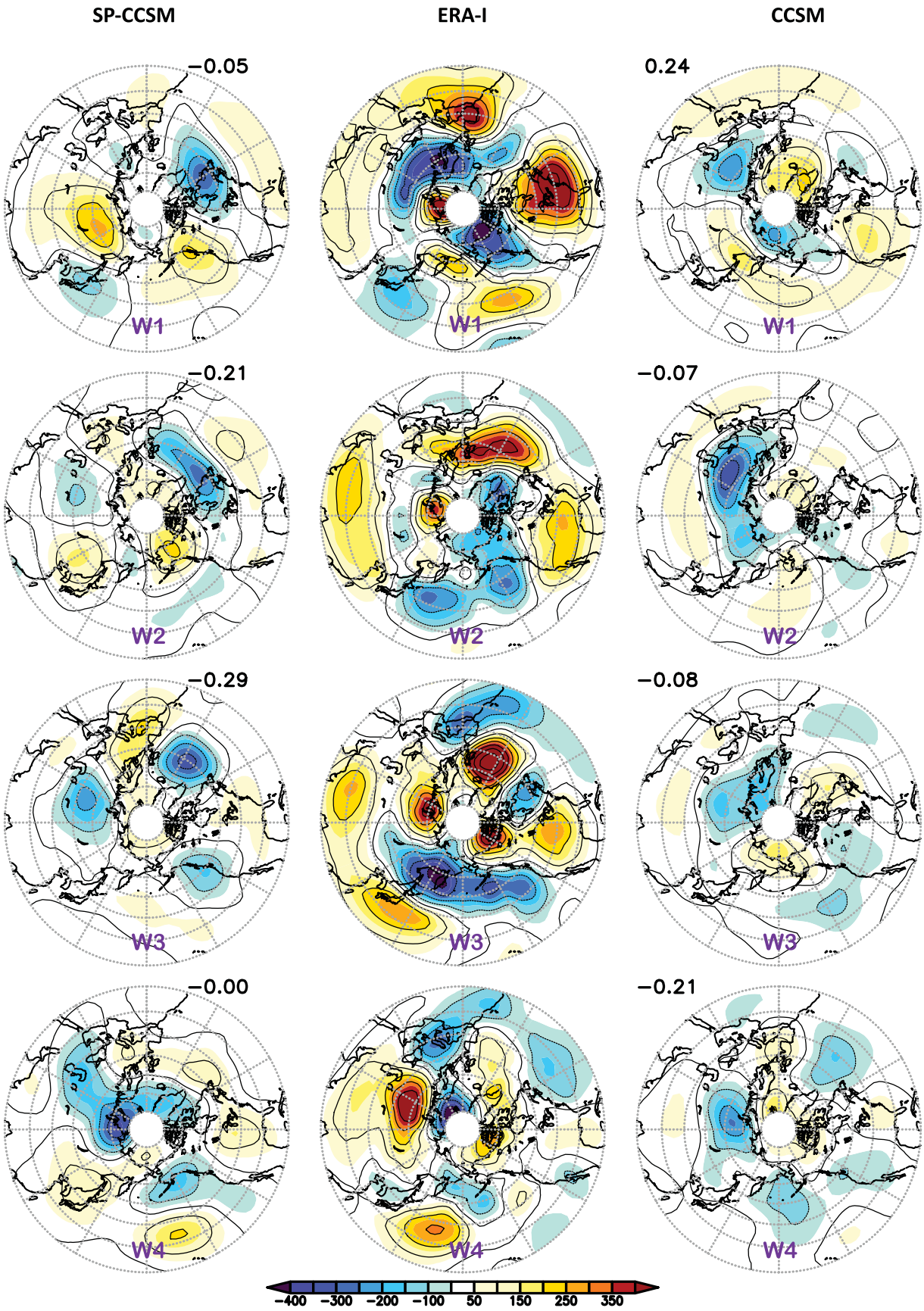

Fig. 8 As in Fig. 7, but for days when active convective activity in observations is located over the Indian Ocean.

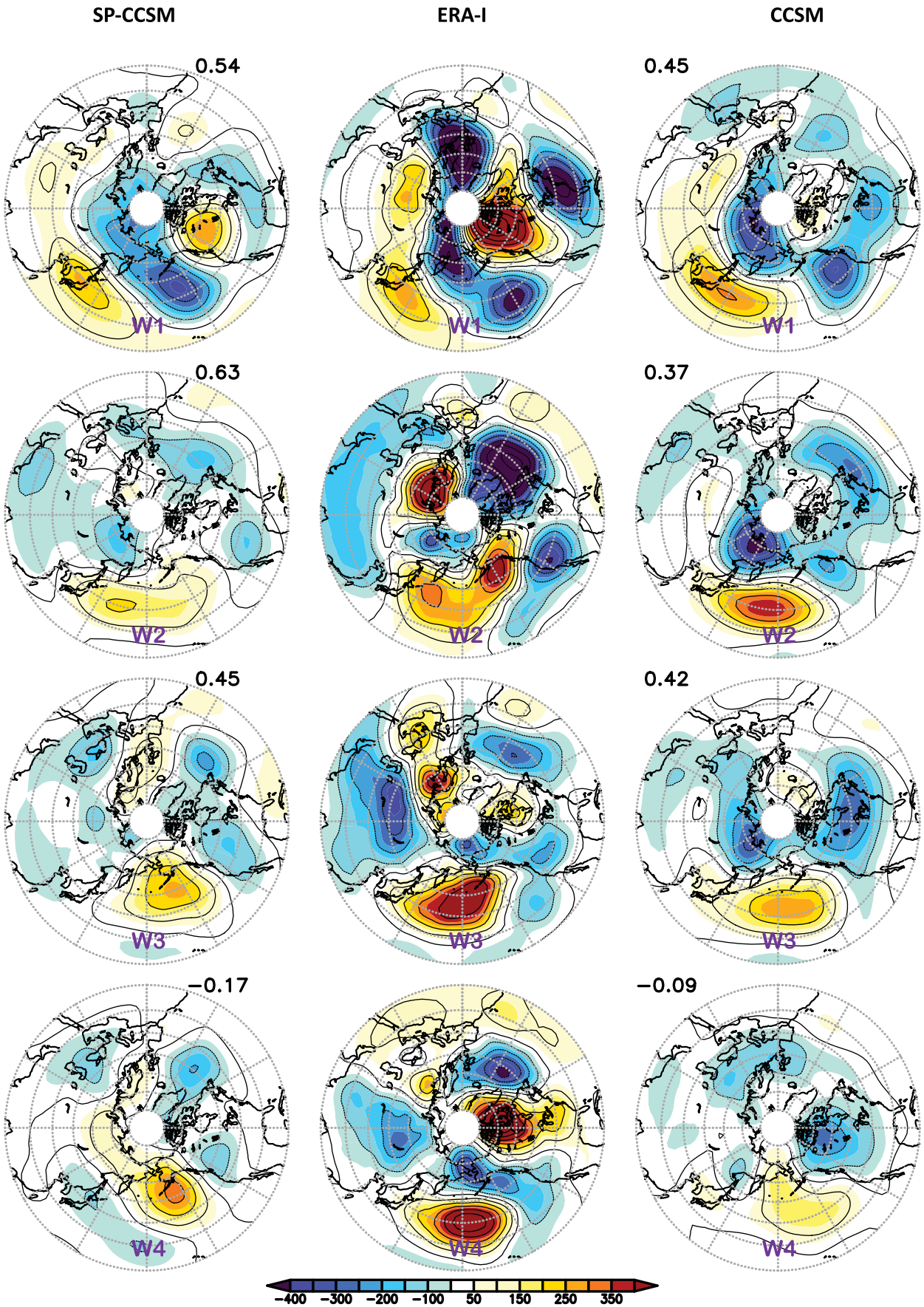

Fig. 9 As in Fig. 7, but for days when active convective activity in the model is located over the western Pacific Ocean.

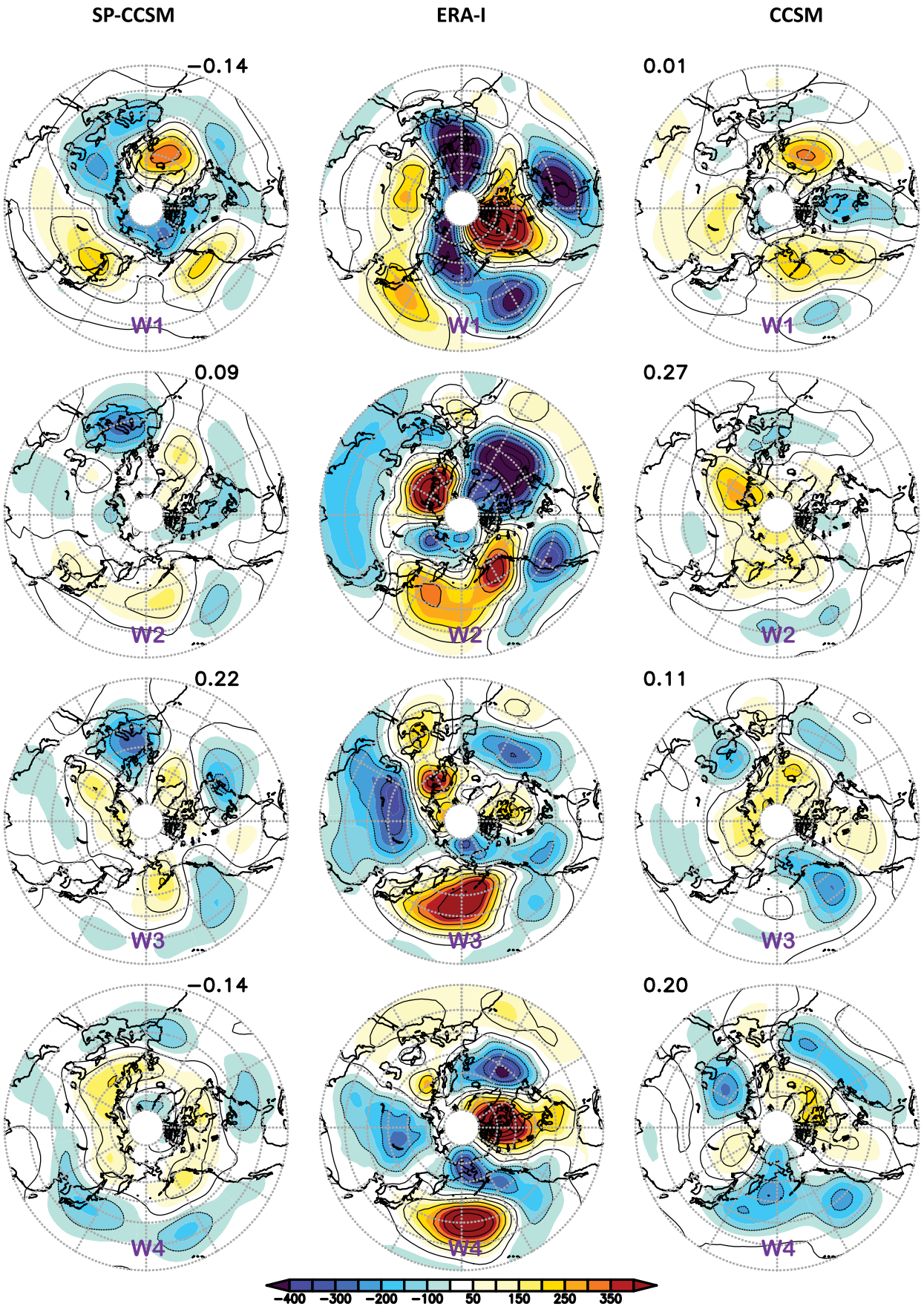

Fig. 10 As in Fig. 7, but for days when active convective activity in observations is located over the western Pacific Ocean.

can lead to large forecast errors in the mid-latitude teleconnection patterns.

For the teleconnection patterns forced by the Indian Ocean convection (Fig. 7), at lead time one week, SP-CCSM shows mid-latitude circulation patterns comparable to observations, whereas the CCSM tends to be dominated mostly by positive anomalies. The positive anomaly over eastern North America and the North Atlantic in the SP-CCSM is weaker than in observations. In the CCSM, this positive centre is slightly stronger than in the SP-CCSM but still weaker than observed and confined over the continent. The SP-CCSM also shows good forecast skill at lead times of two to four weeks for the well-developed NAO+ teleconnection pattern in the observations. In contrast, the CCSM does not forecast the NAO+ phase in the second week. At lead times of three and four weeks, the CCSM re-forecast continues to diverge from the verification and becomes dominated by weak negative anomaly centres.

In the case of mid-latitude teleconnection patterns forced by the MJO convection located over the western Pacific, both models show large differences between the verification using the model-based RMM index (Fig. 9) and observation-based index (Fig. 10). Figure 9 shows that at a lead time of one week, the SP-CCSM model captures the positive height anomaly in the Gulf of Alaska with a magnitude comparable to observations, although shifted. In the CCSM, the anomaly is negative. At longer lead times, the magnitude of the anomaly in the SP-CCSM becomes weaker than in the observations. By week four, in the CCSM the sign of the teleconnection pattern in the Gulf of Alaska is opposite to that in the observations.

The large differences between the composites of the CCSM based on the model RMM index and observations suggest that the large errors noted in the location of convective activity and phase errors have a large impact on the simulation of teleconnection patterns. Likewise, for both models the differences between the model- and observation-based composites show the importance of tropical forcing for the accurate simulation of mid-latitude circulation anomalies. For example, at a lead time of one week both models forecast the general patterns of the mid-latitude variability (Figs 7 and 9). This variability is likely related to the persistence in the initial conditions and driven by the intrinsic variability of the mid-latitudes.

4 Summary and discussion

The impact of cloud representation on the forecast of mid-latitude teleconnections on intra-seasonal time scales was evaluated using an ocean–atmosphere coupled climate model with two approaches for modelling cloud processes. In the first approach, moist convection is represented by a conventional parameterization scheme. In the second approach, cloud processes are quasi-explicitly simulated by a 2D CRM embedded in each grid column of the atmospheric model. The evaluation of a limited ensemble of re-forecasts shows a better deterministic forecast skill for MJO in the model with the super-parameterization representation of cloud processes. The MJO forecast errors have an impact on the forecast skill of mid-latitude teleconnection patterns. The large phase errors in the first week of the CCSM simulation lead to erroneous teleconnection patterns forced by the MJO active convection located in the Indian Ocean. Yadav and Straus (2017) suggested that in observations fast-propagating MJO events (active convective activity takes 10 days or less to propagate from the Indian Ocean into the west Pacific) tend to produce an NAO+ response associated with phases 4 and 5 of the MJO, which may explain the poor forecast skill associated with MJO phases 2 and 3 in the CCSM. The rapid decrease in anomaly correlation in the second week of the CCSM is accompanied by loss of skill in simulating the teleconnection patterns forced by the MJO active convection located in the western Pacific Ocean.

Simulation of recurrent mid-latitude large-scale circulation flow in the Euro-Atlantic and North Pacific sectors, which have been linked to tropical forcings, also shows sensitivity to the representation of cloud processes. Vitart (2017) suggested that model horizontal resolution may affect the strength of the MJO teleconnections over the Euro-Atlantic sector. In this study, the horizontal resolution on which the large-scale circulation is resolved is the same in the two models, and the wave activity flux (Plumb, 1985) at 200 hPa shows no large difference between the two models (not shown).

The results of this study show that the importance of cloud representation demonstrated for the accuracy of climate simulation remains relevant for a model's forecast skill on sub-seasonal time scales. Improvements in the propagation characteristics of MJO convective activity increase the forecast skill of the MJO life cycle and the associated mid-latitude teleconnections along with the large-scale recurrent patterns.

Acknowledgements

We express special thanks to the World Meteorological Organization Subseasonal-to-Seasonal Prediction (S2S) Project for fostering the Teleconnection Sub-project and encouragement to pursue the Year of Tropics-Midlatitudes Interactions and Teleconnections (YTMIT) virtual field campaign.

Disclosure statement

No potential conflict of interest was reported by the author.

Funding

This work was supported by the National Oceanic and Atmospheric Administration (US NOAA NWS) [grant number NA16NWS4680022].

References

Cassou, C. (2008). Intraseasonal interaction between the Madden–Julian Oscillation and the North Atlantic Oscillation. *Nature*, *455*, 523–527.

Cunningham, C. A. C., & Cavalcanti, I. F. D. A. (2006). Intraseasonal modes of variability affecting the South Atlantic convergence zone. *International Journal of Climatology*, *26*, 1165–1180.

Davini, P., von Hardenberg, J., & Corti, S. (2015). Tropical origin influence for the impacts of the Atlantic multidecadal variability on the Euro-Atlantic climate. *Environmental Research Letters*, *10*, 094010. doi:10.1088/1748-9326/10/9/094010

Dee, D. P., Uppala, S. M., Simmons, A. J., Berrisford, P., Poli, P., Kobayashi, S., … Vitart, F. (2011). The ERA-Interim reanalysis: Configuration and performance of the data assimilation system. *Quarterly Journal of the Royal Meteorological Society*, *137*, 553–597.

DeMott, C. A., Stan, C., Branson, M., & Randall, D. A. (2014). Intraseasonal variability in coupled GCMs: The role of ocean feedbacks and model physics. *Journal of Climate*, *27*, 4970–4995.

Ferranti, L., Corti, S., & Janousek, M. (2015). Flow-dependent verification of the ECMWF ensemble over the Euro-Atlantic sector. *Quarterly Journal of the Royal Meteorological Society*, *141*, 916–924.

Ferranti, L., Palmer, T., Molteni, F., & Klinker, E. (1990). Tropical–extratropical interaction associated with the 30–60 day oscillation and its impacts on medium and extended range prediction. *Journal of the Atmospheric Sciences*, *47*, 2177–2199.

Fu, X., Lee, J. Y., Hsu, P. C., Taniguchi, H., Wang, B., Wang, W., & Weaver, S. (2013). Multi-model MJO forecasting during DYNAMO/CINDY period. *Climate Dynamics*, *41*, 1067–1081.

Gent, P. R., Danabasoglu, G., Donner, L. J., Holland, M. M., Hunke, E. C., Jayne, S. R., … Zhang, M. (2011). The Community Climate System Model version 4. *Journal of Climate*, *24*, 4973–4991.

Gottschalck, J., Wheeler, M., Weickmann, K., Viatrt, F., Savage, N., Lin, H., … Higgins, W. (2010). A framework for assessing operational Madden–Julian Oscillation forecasts – A CLIVAR MJO working group project. *Bulletin of the American Meteorological Society*, *91*, 1247–1258.

Grabowski, W. W. (2001). Coupling cloud processes with the large-scale dynamics using the cloud-resolving convection parameterization (CRCP). *Journal of the Atmospheric Sciences*, *58*, 978–997.

Grabowski, W. W. (2004). An improved framework for superparameterization. *Journal of the Atmospheric Sciences*, *61*, 1940–1952.

Hack, J. J. (1994). Parameterization of moist convection in the National Center for Atmospheric Research Community Climate Model (CCSM2). *Journal of Geophysical Research*, *99*, 5551–5568.

Hoskins, B. J., & Karoly, D. J. (1981). The steady linear response of a spherical atmosphere to thermal and orographic forcing. *Journal of the Atmospheric Sciences*, *38*, 1179–1196.

Hudson, D., Marshall, A. G., Yin, Y. H., Alves, O., & Hendon, H. H. (2013). Improving intraseasonal prediction with a new ensemble generation strategy. *Monthly Weather Review*, *141*, 4429–4449.

Jiang, X., Waliser, D. E., Xavier, P. K., Petch, J., Klingaman, N. P., Woolnough, S. J., … Zhu, H. (2014). Vertical structure and physical processes of the Madden–Julian Oscillation: Exploring the key model physics in climate simulations. *Journal of Geophysical Research*, *120*, 4718–4748.

Jung, T., Miller, M. J., & Palmer, T. N. (2010). Diagnosing the origin of extended range forecast error. *Monthly Weather Review*, *6*, 2434–2446.

Kang, I. S., Jang, P. H., & Almazroui, M. (2014). Examination of multi-perturbation methods for ensemble prediction of the MJO during boreal summer. *Climate Dynamics*, *42*, 2627–2637.

Kang, I. S., & King, H. M. (2009). Assessment of MJO predictability for boreal winter with various statistical and dynamical models. *Journal of Climate*, *23*, 2368–2378.

Khairoutdinov, M., & Randall, D. A. (2001). A cloud resolving model as a cloud parameterization in the NCAR community climate system model: Preliminary results. *Geophysical Research Letters*, *28*, 3617–3620.

Khairoutdinov, M., Randall, D. A., & DeMott, C. A. (2005). Simulations of the atmospheric general circulation using a cloud-resolving model as superparameterization of physical processes. *Journal of the Atmospheric Sciences*, *62*, 2136–2154.

Kiladis, G. N., Dias, J., Straub, K. H., Wheeler, M. C., Tulich, S. N., Kikuchi, K., … Ventrice, M. J. (2014). A comparison of OLR and circulation-based indices for tracking the MJO. *Monthly Weather Review*, *142*, 1697–1715.

Kim, H.-M., Webster, P. J., Toma, V. E., & Kim, D. (2014). Predictability and prediction skill of the MJO in two operational forecasting systems. *Journal of Climate*, *27*, 5364–5378.

Knutson, T. R., & Weickmann, K. M. (1987). 30–60 day atmospheric oscillations: Composite life cycles of convection and circulation anomalies. *Monthly Weather Review*, *115*, 1407–1436.

Liebmann, B., & Smith, C. A. (1996). Description of a complete (interpolated) outgoing longwave radiation dataset. *Bulletin of the American Meteorological Society*, *77*, 1275–1277.

Lin, H., Brunet, G., & Derome, J. (2008). Forecast skill of the Madden–Julian Oscillation in two Canadian atmospheric models. *Monthly Weather Review*, *136*, 4130–4149.

Lin, H., Derome, J., & Brunet, G. (2009). An observed connection between the North Atlantic Oscillation and the Madden–Julian Oscillation. *Journal of Climate*, *22*, 364–380.

Michelangeli, P.-A., Vautard, R., & Legras, B. (1995). Weather regimes: Recurrence and quasi stationarity. *Journal of the Atmospheric Sciences*, *52*, 1237–1256.

Neale, R.-B., Richter, J. H., & Jochum, M. (2008). The impact of convection on ENSO: From a delayed oscillator to a series of events. *Journal of Climate*, *21*, 5904–5924.

Park, S., & Bretherton, C. S. (2009). The University of Washington shallow convection and moist turbulence schemes and their impact on climate simulations with the Community Atmosphere Model. *Journal of Climate*, *22*, 3449–3469.

Plumb, A. R. (1985). On the three-dimensional propagation of stationary waves. *Journal of the Atmospheric Sciences*, *42*, 217–229.

Rashid, H., Hendon, H. H., Weehler, M. C., & Alves, O. (2011). Prediction of the Madden–Julian Oscillation with the POMA dynamical prediction system. *Climate Dynamics*, *36*, 649–661.

Richter, J. H., & Rasch, P. J. (2008). Effects of convective momentum transport on the atmospheric circulation in the Community Atmosphere Model, version 3. *Journal of Climate*, *21*, 1487–1499.

Saha, S., Moorthi, S., Pan, Hua-Lu, Wu, X., Wang, J., Nadiga, S., … Goldberg, M. (2010). The NCEP climate forecast system reanalysis. *Bulletin of the American Meteorological Society*, *91*, 1015–1058.

Seo, K. H., Wang, W., Gottschlack, J., Zhang, Q., Schemm, J. K. E., Higgins, W. R., & Kumar, A. (2009). Evaluation of MJO forecast skill from several statistical and dynamical models. *Journal of Climate*, *22*, 2372–2388.

Stan, C., Khairoutdinov, M., DeMott, C. A., Krishnamurthy, V., Straus, D. M., Randall, D. A., … Shukla, J. (2010). An ocean-atmosphere climate simulation with an embedded cloud resolving model. *Geophysical Research Letters*, *37*, L01702. doi:10.1029/2009GL040822

Stan, C., & Xu, L. (2014). Climate simulations and projections with a super-parameterized climate model. *Environmental Modeling and Software*, *60*, 134–152.

Straus, D. M. (2010). Synoptic-eddy feedbacks and circulation regime analysis. *Monthly Weather Review*, *138*, 4026–4034.

Straus, D. M., Corti, S., & Molteni, F. (2007). The link between weather and the large scale circulation. *Journal of Climate*, *20*, 2251–2272.

Straus, D. M., Molteni, F., & Corti, S. (2017). The link between weather and large scale circulation. In C. L. E. Franzke, & T. J. O'Kane (Eds.), *Nonlinear and stochastic climate dynamics* (pp. 105–135). Cambridge, UK: Cambridge University Press.

Thayer-Calder, K., & Randall, D. A. (2009). The role of convective moistening in the Madden–Julian Oscillation. *Journal of the Atmospheric Sciences*, *66*, 3297–3312.

Tseng, K.-C., Barnes, E. A., & Maloney, E. D. (2018). Prediction of the midlatitude response to strong Madden–Julian Oscillation events on S2S time scales. *Geophysical Research Letters*, *45*, 463–470.

Vitart, F. (2014). Evolution of ECMWF sub-seasonal forecast skill scores. *Quarterly Journal of the Royal Meteorological Society*, *140*, 1889–1899.

Vitart, F. (2017). Madden–Julian Oscillation prediction and teleconnections in the S2S database. *Quarterly Journal of the Royal Meteorological Society*, *143*, 2210–2220.

Vitart, F., Ardilouze, C., Bonet, A., Brookshaw, A., Chen, M., Codorean, C., … Zhang, L. (2017). The sub-seasonal to seasonal (S2S) prediction project database. *Bulletin of the American Meteorological Society*, *98*, 163–173.

Vitart, F., & Molteni, F. (2010). Simulation of the MJO and its teleconnections in the ECMWF forecast system. *Quarterly Journal of the Royal Meteorological Society*, *136*, 842–855.

Vitart, F., Woolnough, S., Balmaseda, M. A., & Tompkins, A. M. (2007). Monthly forecast of the Madden–Julian Oscillation using a coupled GCM. *Monthly Weather Review*, *135*, 2700–2715.

Waliser, D. E., Moncrieff, M. W., Burridge, D., Fink, A. H., Gochis, D., B. N. Goswami, … Yuter, S. (2012). The 'year' of tropical convection (May 2008–April 2010): Climate variability and weather highlights. *Bulletin of the American Meteorological Society*, *93*, 1189–1218.

Wang, W., Hung, M. P., Weaver, S. J., Kumar, A., & Fu, X. (2014). MJO prediction in the NCEP climate forecast system version 2. *Climate Dynamics*, *42*, 2509–2520.

Wheeler, M. C., & Hendon, H. H. (2014). An all-season real-time multivariate MJO index: Development of an index for monitoring prediction. *Monthly Weather Review*, *132*, 1917–1932.

Wu, J., Ren, H.-L., Zuo, J., Zhao, C., Chen, L., & Li, Q. (2016). MJO prediction skill, predictability, and teleconnection impacts in the Beijing Climate Center atmospheric general circulation model. *Dynamics of Atmosphere and Oceans*, *75*, 78–90.

Xavier, P. K., Petch, J. C., Klingaman, N. P., Woolnough, S.J., Jiang, X., Waliser, D. E., … Wang, H. (2015). Vertical structure and physical processes of the Madden–Julian oscillation: Biases and uncertainties at short range. *Journal of Geophysical Research*, *120*, 4749–4763.

Yadav, P., & Straus, D. M. (2017). Circulation response to fast and slow MJO episodes. *Monthly Weather Review*, *145*, 1577–1596.

Zappa, G., Masato, L., Woollings, K., & Hodges, K. (2013). Linking northern hemisphere blocking and storm track biases in the CMIP5 climate models. *Geophysical Research Letters*, *41*, 135–139.

Zhang, G. J., & McFarlane, N. A. (1995). Sensitivity of climate simulations to the parameterization of cumulus convection in the Canadian Climate Centre general circulation model. *Atmosphere-Ocean*, *33*, 407–446.